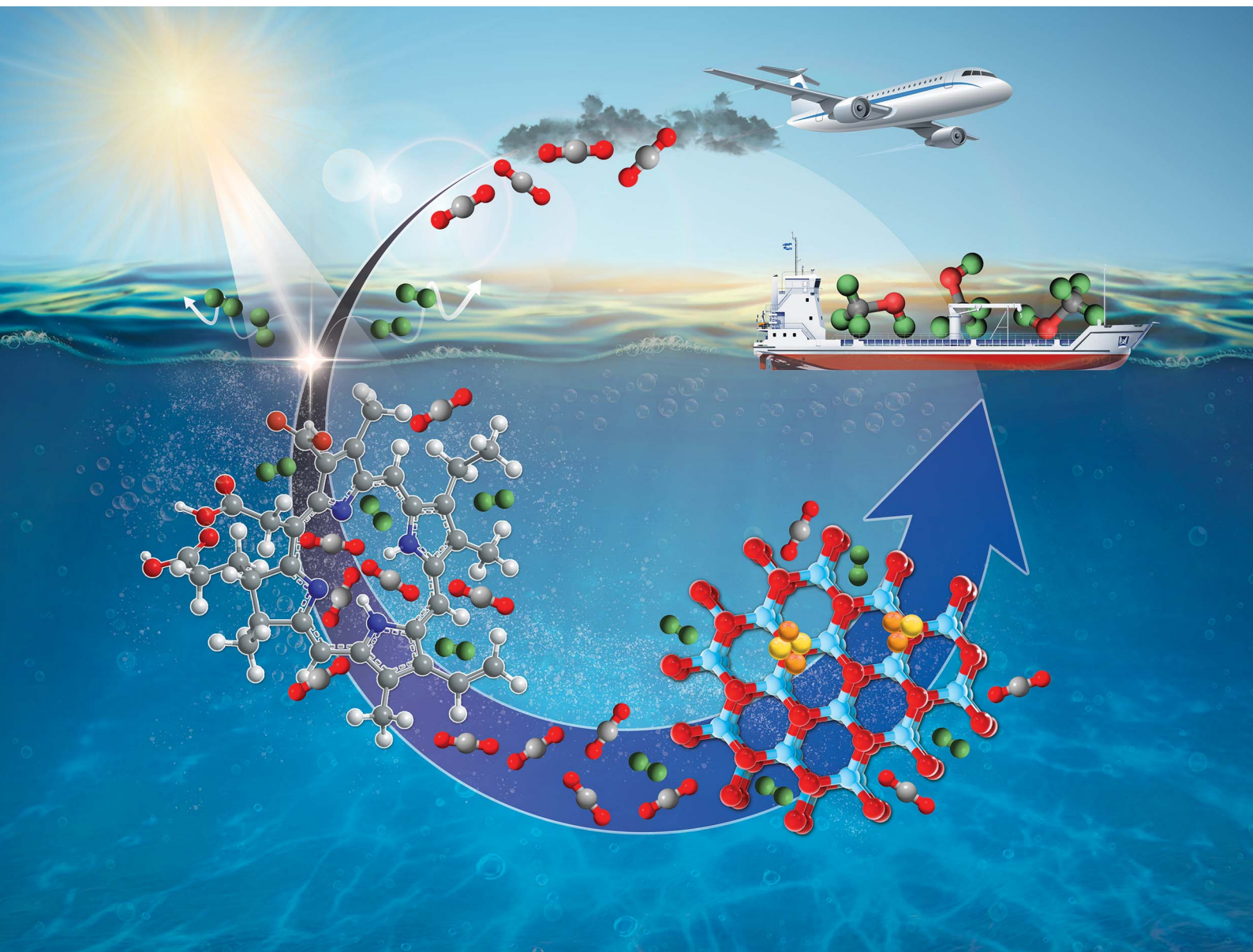


Journal of Materials Chemistry A

Materials for energy and sustainability

rsc.li/materials-a



ISSN 2050-7488

COMMUNICATION


Ali M. Abdel-Mageed *et al.*
A porphyrin co-catalyst enhancing low-temperature CO₂
hydrogenation at the water-Cu_xAu/ZnO interface

Cite this: *J. Mater. Chem. A*, 2025, **13**, 30929Received 10th April 2025
Accepted 24th June 2025

DOI: 10.1039/d5ta02862k

rsc.li/materials-a

A porphyrin co-catalyst enhancing low-temperature CO₂ hydrogenation at the water–Cu_xAu_y/ZnO interface†

Hung Mac,^a Katja Neubauer,^a Thanh Huyen Vuong,^a M. Parlinska-Wojtan^b and Ali M. Abdel-Mageed  ^{*a}

The activation of CO₂ at the liquid/solid interface is highly promising for various catalytic processes and applications, offering the significant advantage of reduced mass and heat transfer effects compared to gas/solid interface. Considering water as a green reaction medium, this process is particularly challenged by the limited solubility of CO₂ and H₂ leading to low hydrogenation rates. Herein, we demonstrated that a water-soluble porphyrin derivative, chlorophyllin complex, can act as a co-catalyst for the conversion of CO₂ to methanol in water on CuAu/ZnO catalysts. While chlorophyllin itself is catalytically inactive, its presence increases the water solubility of reaction gases leading to up to a 3-fold increase in CO₂ conversion at 160 °C, while maintaining high selectivity toward methanol. Zeta potential results suggest electrostatic interactions between CO₂ and chlorophyllin, enhancing solubility. Spin trap-assisted EPR spectroscopy indicated the formation of C-center and OH radicals during the reaction, with their concentration increasing in the presence of chlorophyllin. These results represent a further step towards enabling the capture and hydrogenation of CO₂ at liquid/solid interfaces.

Introduction

Using the greenhouse carbon dioxide gas as a building block to produce chemicals and fuels can reduce dependence on fossil fuels, lowering the carbon footprint and eventually achieving a zero-carbon cycle.¹ Converting CO₂ to methanol is particularly desirable, as it shares several characteristics with oil, making it an ideal energy storage and transport medium.^{2,3} Methanol is particularly advantageous because it is liquid under ambient conditions and, additionally, can serve as a platform for a wide range of chemical conversions.⁴ The success of this strategy largely depends on the development of catalysts that can

selectively convert CO₂ into methanol with high activity. Performing CO₂ hydrogenation in the liquid phase on the surface of solid heterogeneous catalysts (*i.e.*, at the liquid(gas)/solid interface) is particularly attractive approach from both technical and fundamental perspectives. On one hand, this process is highly favorable in terms of process safety, the easy control of mass diffusion and the efficient heat dissipation and spread of hot spots in the catalyst bed during reaction.⁵ Additionally, the dissolving power of specific solvent for liquid products, such as methanol, can help shift the reaction equilibrium towards the product.⁶ Optimizing and understanding this process in the liquid phase are also highly beneficial for other related research and technological areas, such as the photocatalytic reduction of CO₂, which is primarily conducted in aqueous media,⁷ CO₂ capture in liquid amines,⁸ and electrochemical CO₂ activation.⁹

We recently reported on the potential for CO₂ reduction in the liquid phase using water as a green solvent on heterogeneous Cu_xAu_y/ZnO catalysts, which contain a relatively low concentration of Au (≤ 7 mol%).¹⁰ These catalysts showed selectivity for methanol in the liquid phase between 96 and 100% in the temperature range between 200 and 240 °C at 50 bar. Comparable product selectivities were obtained under flow conditions at gas/solid interfaces.¹¹ This process is often studied in organic solvents, which, despite higher CO₂ conversion, are impractical due to the potential reaction of CO₂ products with these solvents^{9–14} and additionally the need for intensive processing steps.¹² The successful industrial applications require excellent control over product selectivity, ideally yielding a single product (*e.g.*, methanol) to minimize costly separation steps. In CO₂ reduction to methanol, CO formation can be avoided by operating at lower temperatures (< 200 °C).¹³ This would lead, however, to limited reaction rates. In the liquid phase, particularly in water, the reaction is additionally challenged by the limited gas solubility at temperatures relevant to CO₂ hydrogenation, which requires the application of extremely high pressures and much lower temperatures. A water-soluble mediator that increases gas solubility in water could enhance

^aLeibniz Institute for Catalysis (LIKAT), D-18059 Rostock, Germany. E-mail: ali.abdelmageed@catalysis.de^bInstitute for Nuclear Physics, Polish Academy of Sciences, 31342 Krakow, Poland† Electronic supplementary information (ESI) available. See DOI: <https://doi.org/10.1039/d5ta02862k>

activity at lower temperatures. Enhanced gas solubility at low temperatures is, thus, key to efficient CO₂ hydrogenation.

Inspired by the natural interaction of the porphyrin molecular species such as chlorophyllin molecules with CO₂ and H₂O in photosynthesis, we hypothesized that it could act as a macromolecular mediator to enhance the solubility of gas reactants in water, thus increasing their accessibility to active surface sites of Cu_xAu_y/ZnO catalysts. Among different available analogues of chlorophyll molecules featuring different ion centers such as Mg²⁺ or Cu²⁺, we selected a Cu-based and water-soluble porphyrin complex. We investigated the effect of varying amounts of the porphyrin complex (chlorophyllin) on reactant gas solubility in water and its impact on low-temperature CO₂ hydrogenation to methanol, using ZnO-supported Cu_xAu_y nanoalloys, which have previously shown promising results for CO₂ hydrogenation in both the liquid and gas phases. Building on our previous results,¹⁰ the current findings demonstrate that CO₂ conversion in the presence of chlorophyllin in aqueous medium can occur at much lower temperatures (160 °C), while maintaining conversion levels comparable to those at 200 °C. This lower reaction temperature helps to thermodynamically suppress the undesired CO formation *via* the reverse water–gas shift reaction, thus increasing methanol formation rates.

Results and discussion

Based on the reported findings on bimetallic Cu_xAu_y/ZnO catalysts¹⁰ as well as the detailed studies on monometallic Au/ZnO catalysts,^{14–16} we prepared 3 different Cu_xAu_y/ZnO catalysts with total Cu + Au loadings between 3.0 and 20 wt% (see Table S1†). The Au content was kept at ≤5 mol%, which is known to have the highest activity and selectivity for methanol at both gas/solid¹⁰ and liquid(gas)/solid interfaces.¹² In this contribution, we performed selected characterization studies, including powder X-ray diffraction (PXRD) and electron microscopy (see detailed structural elucidation in ref. 10 and 12). We examined the samples using electron microscopy to assess the reproducibility of Cu_xAu_y nanoparticles compared to previous studies. 3 and 10 wt% loadings resulted in comparable average particle sizes of 4.1 ± 1.4 and 4.4 ± 1.9 nm, respectively (see Fig. 1). The highest loading showed a slight shift to larger sizes (5.4 ± 2.0 nm), still close to lower loadings. These particle size distributions align well with earlier results using the same procedure. The *ex situ* PXRD shown in Fig. S1† exhibited diffraction peaks belonging to ZnO wurtzite crystals together with diffraction peaks related to oxidic Cu species, CuO_x (35.45°, 38.68°)¹⁷ and CuAu (42.62°, 48.96°) alloy,¹⁸ in agreement with previous findings.¹⁰

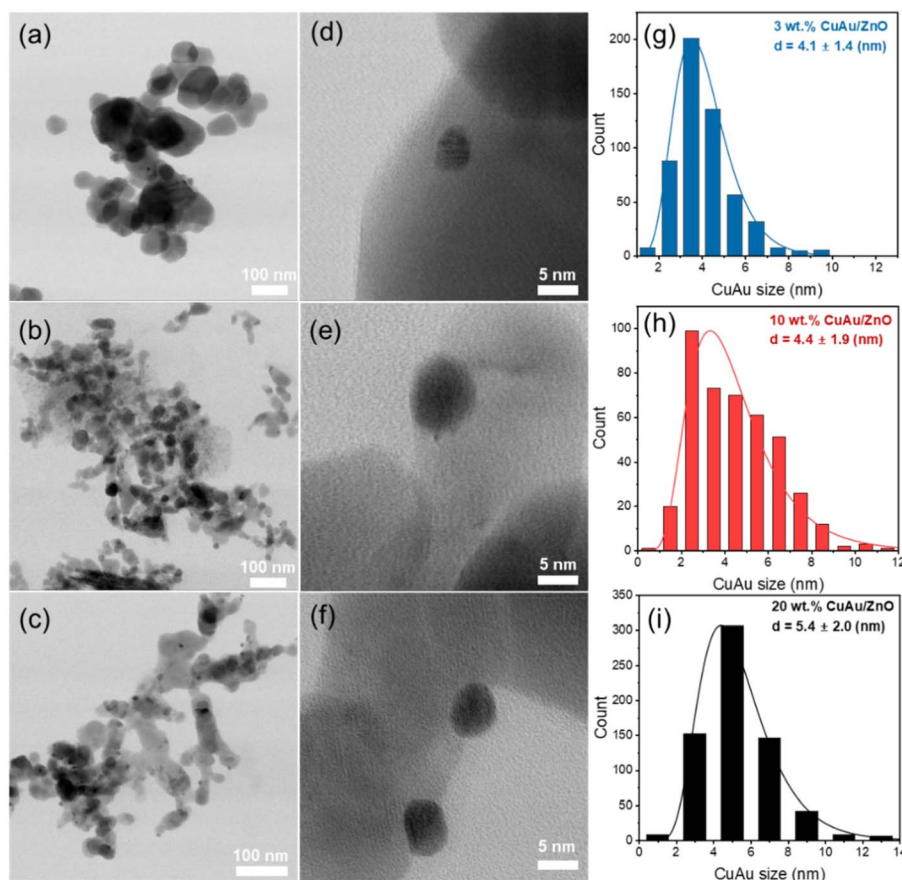


Fig. 1 Representative STEM micrographs of different loadings of the Cu_xAu_y alloy (3, 10, and 20 wt%) on a ZnO support. Overview images (a–c) and high-resolution images of Cu_xAu_y alloy nanoparticles (d–f), and corresponding particle size distributions (g–i).



At this point, and before examining the catalytic behavior, we first investigated the effect of the concentration of a water-soluble Cu-based chlorophyllin complex (see the structure in Fig. 2a) on the solubility of CO₂ in water, which is also expected to scale up with the solubility of H₂. To do this, we pressurized 12 bar of CO₂ in water containing different concentrations of chlorophyllin under 12 bar of pure CO₂ and then examined the solubility of CO₂ in water after equilibrium was reached at room temperature. Changes in CO₂ solubility were examined by monitoring the chromatographic peak of CO₂ in the solution using GC-MS (see Fig. 2b and the experimental section in the ESI†). As the concentration of chlorophyllin in water increased, we observed a rise in the intensity of water-soluble CO₂ (GC-MS-integrated peak area), reaching a maximum at 0.01 g_{chlorophyllin} L⁻¹. Further increase of chlorophyllin concentration gradually decreased CO₂ peak intensity, reaching its lowest at 4 g_{chlorophyllin} L⁻¹.

For easy and quantitative interpretation, we plotted relative intensity, defined as the peak area at a specific concentration divided by the largest peak area obtained at 0.01 g_{chlorophyllin} L⁻¹ (see absolute intensities in Fig. S2†). This results in a volcano-shaped dependence of CO₂ solubility on chlorophyllin concentration, peaking at 0.01 g_{chlorophyllin} L⁻¹ (Fig. 2c). Notably, CO₂ solubility remained higher in all chlorophyllin solutions than in chlorophyllin-free water. This increase is likely due to interactions between CO₂ and nitrogen atoms in the framework of porphyrin molecules.¹⁹ Another scenario involves the interaction of anionic CO₂ species with the

porphyrin complex. Note that CO₂, a weak acidic gas, produces conjugate anions upon dissolution in water, including HCO₃⁻ and CO₃²⁻, which can interact electrostatically with Cu²⁺, helping to increase CO₂ capture in the liquid phase. The reduced CO₂ solubility at high chlorophyllin concentrations may be due to CO₂ competing for binding sites of chlorophyllin molecules and/or steric effects from excess chlorophyllin in water.

The change in pH of the reaction medium was examined for water and chlorophyllin-containing water after CO₂ pressurization (see Fig. 2d). For water, CO₂ reduced the pH from 7.3 to 6.0, while for chlorophyllin solution, the pH dropped from 8.2 to 5.6. This suggests that the porphyrin complex increased water's basicity. More notably, the pH decline in the chlorophyllin solution (31.7%) was greater than in neutral water (17.8%). This correlates with the significant increase in CO₂ solubility in the chlorophyllin mixture, indicating that the porphyrin complex enhances water's ability to capture CO₂. Finally, given the chlorophyllin-mediated increase in CO₂ solubility in water, a similar trend for H₂ can be assumed. H₂ is reported to interact with metal porphyrin complexes such as chlorophyllin.²⁰ Quantifying this effect for H₂ at these temperatures is, however, currently not feasible and remains open for future investigations.

Next, we studied the catalytic CO₂ hydrogenation (35 bar H₂ + 15 CO₂) performance of selected Cu_xAu_y/ZnO catalysts (≤5 mol% of Au – see Table S1†) in water and in water containing 0.01 g_{chlorophyllin} L⁻¹ at 160 °C. In the absence and

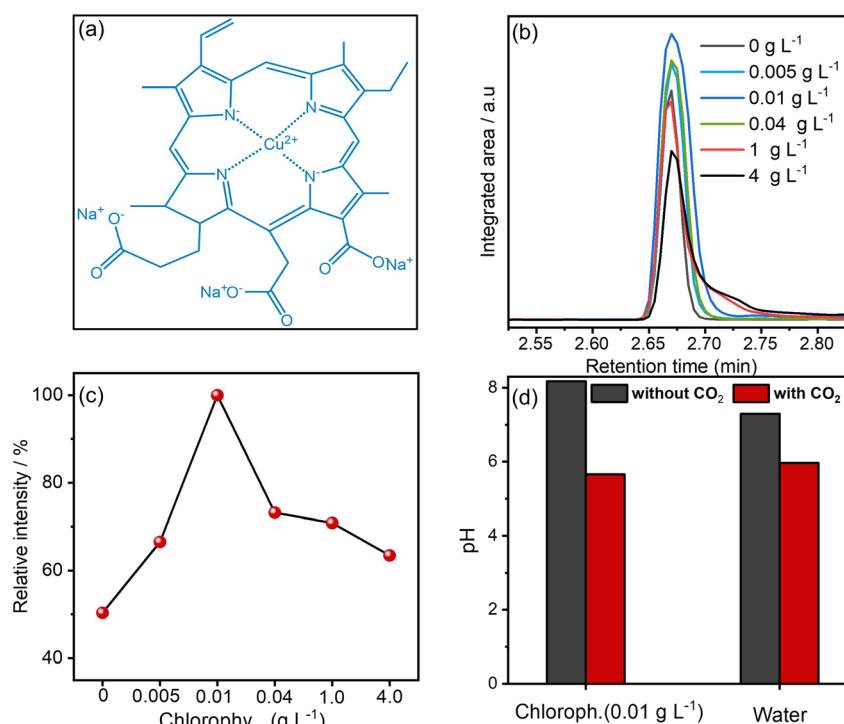


Fig. 2 (a) The chemical structure of the Cu-based chlorophyllin (porphyrin molecule). (b) The GC-MS peak of soluble CO₂ in water for different concentrations of chlorophyllin in water (12 bar CO₂ pressurized in pure water or in the chlorophyllin mixture at 25 °C for 18 h before measuring concentration in water). (c) Plot of the relative intensity of CO₂ peaks (R_i = GC-MS peak area at a specific concentration/GC-MS peak area at 0.01 g_{chlorophyllin} L⁻¹). (d) pH of pure water and water containing chlorophyllin (0.01 g_{chlorophyllin} L⁻¹) solutions in the absence and the presence of CO₂.



presence of chlorophyllin, only methanol was detected as the product, with no side gas products (e.g., CO or CH₄) observed (GC-MS data in Fig. S3 and S4†). CO₂ conversion in water was 0.71%, 1.67%, and 0.83% for 3, 10, and 20 wt% Cu_xAu_y/ZnO catalysts (Fig. S5a† and GC-MS data in Fig. S6†), which increased in the presence of chlorophyllin to 2.12%, 3.29%, and 2.54%, respectively (Fig. S5b†). Carbon balance was calculated based on gas and liquid phase analysis, where a maximum carbon loss of ≤3% was quantified (see ESI, Section 2.7†). The productivity of methanol formation upon introduction of chlorophyllin increased by 2–3 times, depending on the loading of the Cu_xAu_y nanoalloy, with the highest catalyst mass-normalized activity observed on the 10 wt% Cu_xAu_y/ZnO catalyst (see Fig. 3a and b). The magnitude of improvement of methanol productivity in the presence of chlorophyllin was found to increase with decreasing total metal loading (Cu + Au), as shown in Fig. 3c. Product formation (methanol) and potential side products were additionally verified by ¹H NMR spectroscopy in the reaction liquid, excluding any side products under the present conditions (Fig. S7 and S8†). For benchmarking, we compared the present results, obtained at 160 °C, with earlier findings obtained at higher reaction temperature.¹⁰ The results showed that methanol productivity in the case of using chlorophyllin as a co-catalyst at 160 °C is equal to or even higher than that obtained at a temperature of 200 °C, while maintaining high selectivity towards methanol at 160 °C (see Fig. 3d). The thermodynamic tendency for CO formation *via* reverse-water-gas-shift (RWGS: CO₂ + H₂ → CO + H₂O) is inherently (almost completely) suppressed.²¹

To determine whether the observed enhancement is due to independent effects on reaction kinetics for the liquid dispersed Cu_xAu_y/ZnO catalyst and chlorophyllin, we examined the activity of chlorophyllin toward CO₂ hydrogenation without the Cu_xAu_y/ZnO catalysts. Catalytic testing with a chlorophyllin solution (0.01 g_{chlorophyllin} L⁻¹ at 160 °C/50 bar) alone showed no methanol formation (see NMR data in Fig. S9†). This suggests that the porphyrin complex alone is inactive under the present conditions. Other possible effects such as altering catalyst activity or boosting hydrogen solubility, particularly at lower temperatures, cannot be excluded and require further scrutiny. Overall, improved CO₂ solubility at low temperatures *via* chlorophyllin can lower the reaction temperature and costs, while also helping to suppress the unwanted RWGS reaction.

Finally, we examined the impact of the amount of Au in the Cu_xAu_y/ZnO catalysts on activity and product selectivity in the presence of chlorophyllin. The results show that CO₂ conversion and product distribution depend strongly on the gold-to-copper ratio. We observed that increasing the gold content to 41 mol% shifted the product selectivity (see results in Fig. S10† and NMR spectra in Fig. S11 and S12†), predominantly from methanol to primarily formic acid (96% formic acid and 4% methanol). Further increasing the gold content to 75 mol% resulted in a decrease in CO₂ conversion and a reduction in formic acid selectivity to 79%, with 21% selectivity to methanol.

To investigate the role of chlorophyllin on the activity of Cu_xAu_y/ZnO catalysts for CO₂ hydrogenation, and whether it only enhances CO₂ solubility or it induces additionally other effects on the catalyst surface, we examined the catalyst surface post-reaction using transmission FTIR spectroscopy. A

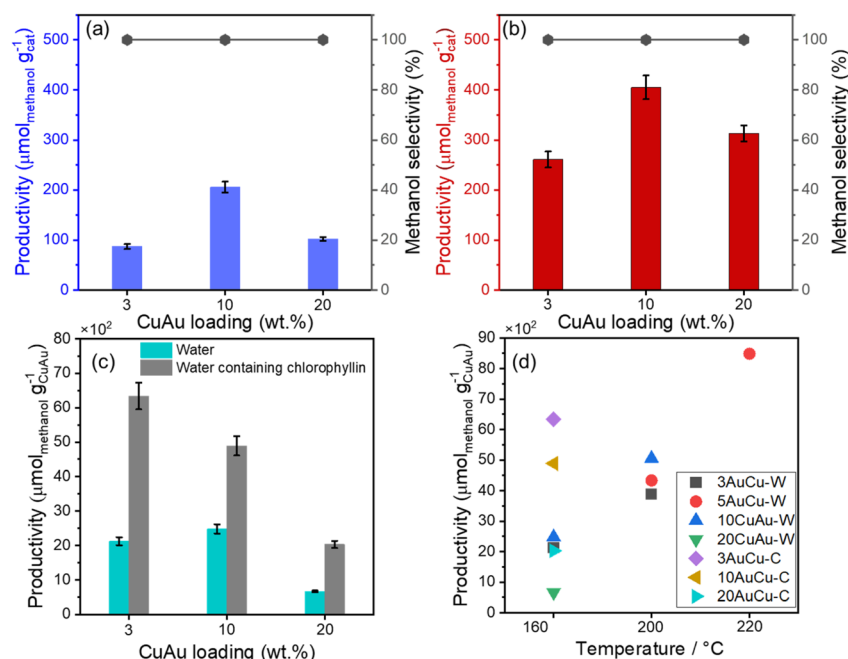


Fig. 3 Methanol productivity and selectivity from CO₂ reduction (35 bar H₂ + 15 CO₂) (a) in water and (b) in water containing chlorophyllin (0.01 g_{chlorophyllin} L⁻¹) at 160 °C on Cu_xAu_y/ZnO catalysts different in total metal loadings (3, 10 and 20 wt%). (c) Metal mass/normalized methanol productivity in water and water containing chlorophyllin. (d) Methanol productivity during CO₂ reduction on Cu_xAu_y/ZnO catalysts in water (W) and water containing chlorophyllin (C) at different temperatures.



comparison of spectra before and after the reaction showed no evidence of chlorophyllin immobilization on the surface (see spectra in Fig. S13†). Interestingly, we observed in the FTIR spectra signals at 1462, 1383, 862, and 738 cm^{-1} characteristic of surface carbonate species on $\text{Cu}_x\text{Au}_y/\text{ZnO}$ catalysts.²² The formation of surface carbonate species was previously observed during methanol synthesis from CO_2/H_2 under flow conditions, despite not being considered as an active reaction intermediate.²³ The intensity of these peaks is more pronounced in the presence of chlorophyllin during the reaction. This observation would agree qualitatively with the limited loss in CO_2 balance during reaction, as mentioned before ($\leq 3\%$).

We further confirmed these results by analyzing the pristine and spent $\text{Cu}_x\text{Au}_y/\text{ZnO}$ samples using energy dispersive X-ray spectroscopy coupled with scanning electron microscopy (SEM-EDX). The results showed that the carbon content on the surface of the spent catalyst with chlorophyllin was 23.5 wt%, higher compared to the chlorophyllin-free mixture (see Fig. S14–S16 and Table S2†). These observations agree with the increase of the ZnCO_3 signal observed in the FTIR spectra.

Next, we studied the pH dependence of the zeta potential of the catalyst surface in the presence and absence of chlorophyllin, for both CO_2 -free and CO_2 -saturated reaction liquid. These experiments aimed to assess the impact of CO_2 and chlorophyllin on the surface charge of $\text{Cu}_x\text{Au}_y/\text{ZnO}$ catalyst particles. The pH range was limited to 10 to prevent ZnO leaching. We observed irregular zeta potential behavior for the

pure water sample without CO_2 , from a pH of 2 to around 6.8, with a maximum at a pH of 3 (23 mV), followed by a decrease before and after this point. At pH 7, the zeta potential reached zero, corresponding to the isoelectric point (IEP). Upon exceeding the IEP value and increasing the pH to 10, the zeta potential was found to decrease continuously, reaching about -28 mV at pH 10. In the chlorophyllin solution, the zeta potential remained negative across the entire pH range, except near pH 3.4, corresponding to the IEP value. For CO_2 -saturated water, the zeta potential was more negative between pH 10 and 6 compared to CO_2 -free water. In the CO_2 -saturated chlorophyllin-water solution, the zeta potential was -40 mV at pH = 10, increasing as pH decreased, and reached about 4 mV at pH = 2. The IEP values of the catalyst in chlorophyllin and CO_2 -saturated water were 2.6 and 5.0, respectively.

The comparison of the different IEP values shows that CO_2 decreases the IEP value of the $\text{Cu}_x\text{Au}_y/\text{ZnO}$ catalyst surface in water. This decrease is more pronounced in the presence of chlorophyllin. A decrease of the IEP value upon introducing chlorophyllin indicated that the catalyst surface becomes intrinsically more negatively charged. Here, a larger concentration of protons (H^+ cations) is needed to neutralize the catalyst surface to reach the IEP (*i.e.*, zero surface charge). It can thus be inferred that for catalyst samples having lower IEP values there are intrinsically a larger number of negatively charged sites, which are able to interact with the acidic CO_2 molecule. The decrease of the IEP is more pronounced in the

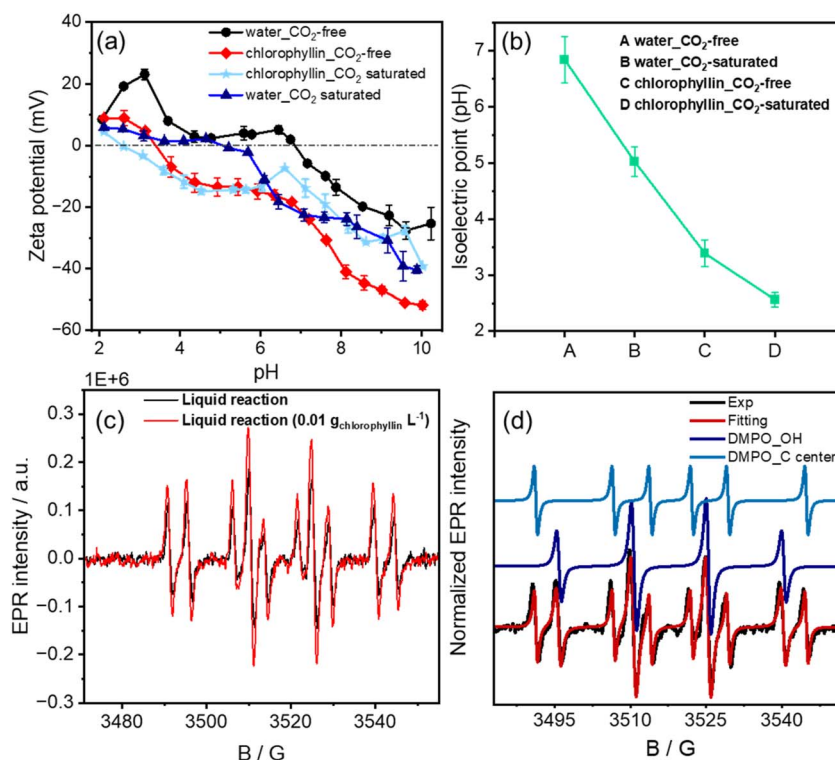


Fig. 4 (a) Zeta potential and (b) isoelectric point (IEP) of the 3 wt% $\text{Cu}_x\text{Au}_y/\text{ZnO}$ catalyst in water and in chlorophyllin for CO_2 -free and CO_2 saturated mixtures and (c) EPR spectra of the reaction mixture in water and water containing chlorophyllin ($0.01 \text{ g}_{\text{chlorophyllin}} \text{ L}^{-1}$) during the CO_2 hydrogenation reaction in the presence of DMPO, and (d) experimental and simulated EPR spectra of DMPO spin trap adducts in the presence of chlorophyllin and simulated components DMPO-OH and DMPO-C-centered adducts.



presence of chlorophyllin, which means that the porphyrin complex presumably helps to mediate the electrostatic interaction of CO_2 with the solid catalyst surface. It should be noted that the reported zeta potentials of ZnO materials are nearly equal or slightly larger than $\text{pH} = 7$,^{24–26} which are higher than our values on $\text{Cu}_x\text{Au}_y/\text{ZnO}$ catalysts. Essentially, the relatively lower IEP in the case of $\text{Cu}_x\text{Au}_y/\text{ZnO}$ catalysts can be explained by the more reduced state of ZnO loaded with metal nanoparticles. Based on previous studies, oxygen vacancy defects are more easily formed in ZnO for Au/ZnO than for Au-free ZnO.^{15,16,27,28} The formation of these point defects increases the surface charge particularly at the metal–ZnO interface, which would agree with the relatively lower IEP in the present case study, especially in the presence of the porphyrin complex.

Finally, we employed spin-trap assisted electron paramagnetic resonance (EPR) spectroscopy to identify the formation of any radical species produced during the CO_2 hydrogenation reaction in water in the presence and in the absence of chlorophyllin. We examined the reaction liquid in water and water containing chlorophyllin ($0.01 \text{ g}_{\text{chlorophyllin}} \text{ L}^{-1}$). After reaction for 5 h, we introduced 5,5-dimethyl-1-pyrroline *N*-oxide (DMPO), as a spin trap for possible radical species formation. Fig. 4c shows the EPR spectra obtained after adding DMPO at room temperature to the two reaction solutions. We observed the characteristic peaks of two DMPO-adduct radicals in both reaction solutions, which are clearly more pronounced in the presence of chlorophyllin. The simulated signals in Fig. 4d can be assigned to the two basic radical species. The first is the DMPO–OH adduct with the hyperfine coupling constants $A_{\text{N}} = 14.91 \text{ G}$ and $A_{\text{H}} = 14.94 \text{ G}$,²⁹ and the second is related to a carbon-centered radical DMPO adduct with $A_{\text{N}} = 15.39 \text{ G}$ and $A_{\text{H}} = 22.67 \text{ G}$.³⁰ The hydroxyl radical ($\cdot\text{OH}$) can be formed by O–H bond dissociation of water on the catalyst³¹ and probably as an intermediate during hydrogenation. Interestingly, the EPR parameters of the DMPO–C-centered adduct closely resemble those of the DMPO– $\text{CO}_2^{\cdot-}$ or DMPO–COOH adduct, known to be formed from the electrochemical CO_2 reduction reaction.³² Therefore, it can intuitively be assumed that the interaction of CO_2 with the $\text{Cu}_x\text{Au}_y/\text{ZnO}$ catalyst surface presumably generates CO_2 radicals during the reaction. Overall, it can be inferred that both CO_2/C -centered and OH radicals are formed under reaction conditions and their concentration is more pronounced in the presence of chlorophyllin during the reaction. This may fit with the observed higher concentration of CO_2 in water in the presence of the chlorophyllin complex. Therefore, it can be concluded that these species are relevant to the dominant CO_2 hydrogenation reaction pathway.

Experimental

Chemicals

Gold(III) chloride trihydrate ($\geq 99.9\%$), copper nitrate trihydrate ($\geq 98\%$), zinc nitrate hexahydrate ($\geq 98.0\%$), sodium carbonate ($\geq 99.5\%$), and sodium hydroxide ($\geq 97\%$) were purchased from Sigma-Aldrich. All the chemicals were used directly without additional purification, and distilled water was used for all experiments.

Preparation of the ZnO support

The ZnO support was synthesized *via* the precipitation method. Two aqueous solutions of $\text{Zn}(\text{NO}_3)_2 \cdot 6\text{H}_2\text{O}$ (0.1 M, 200 mL) and Na_2CO_3 (0.12 M, 200 mL) were prepared in two separate beakers at 70°C . Then, the aqueous $\text{Zn}(\text{NO}_3)_2 \cdot 6\text{H}_2\text{O}$ solution was poured into an aqueous solution of Na_2CO_3 under vigorous stirring at 70°C . The suspension was aged at 70°C for 1 h, and subsequently washed and filtered with distilled water (40°C), until the pH of the supernatant reached a stable value. The resulting precipitate was dried at 80°C overnight and finally calcined in air at 500°C for 4 h.

Synthesis of bimetallic $\text{Cu}_x\text{Au}_y/\text{ZnO}$ catalysts

ZnO (1.0 g) was dispersed in 50 mL of distilled water at 60°C . The pH of the suspension was adjusted to 8–9 using a 1 M NaOH aqueous solution. The bimetallic aqueous solution of Au^{3+} ($\text{HAuCl}_4 \cdot 3\text{H}_2\text{O}$) and Cu^{2+} ($\text{Cu}(\text{NO}_3)_2 \cdot 3\text{H}_2\text{O}$) was added dropwise into the mixture, while maintaining the pH of the resulting mixture at 7.0 by adding dropwise 1 M NaOH solution. Once the solution of Au and Cu precursors was completely added, the suspension was stirred at 60°C for 3 h. The solution was then cooled to room temperature, and the resulting precipitate was washed and filtered with distilled water five times at 40°C . The precipitate was dried at 80°C overnight and subsequently reduced in a 10% H_2/N_2 flow (a total flow rate of 100 mL min^{-1}) with a ramp rate of 5°C min^{-1} to 500°C , where it was held for 2 h.

Catalytic activity measurements and analysis

Analysis of the solubility of CO_2 . The solubility of CO_2 in water containing different concentrations of chlorophyllin was measured using GC-MS (GCMS – GP2010 Ultra, Shimadzu). A glass tube was filled with 5 mL of a 0.01 g per L chlorophyllin solution and placed into a 45 mL Parr stainless steel autoclave. The autoclave was purged with argon at 20 bar pressure three times to ensure the complete removal of air, followed by three additional purges with CO_2 . Finally, the reactor was pressurized with 12 bar of CO_2 and left for 18 hours at 25°C . Afterward, the liquid was injected into the GC-MS to measure the amount of CO_2 absorbed in the chlorophyllin solution.

Catalytic activity experiments. Measurements were carried out in liquid phase batch reactors using 45 mL Parr stainless steel autoclave reactors. The measurement procedure was as follows: 100 mg of catalyst was dispersed in 5 mL of distilled water in a glass tube housed inside autoclave reactors. The charged autoclaves were then purged with Ar at 20 bar three times to ensure the complete removal of any residual oxygen. The reactor was purged again twice with H_2 , followed by pressurization to 50 bars with a CO_2/H_2 (1 : 3) gas mixture. After that, the reactor was heated from room temperature to 160°C at a rate of $10^\circ\text{C min}^{-1}$ under low-speed stirring (150 rpm). Once the thermal equilibrium was achieved, the stirring speed was increased to 1500 rpm, and the reaction time started. At the end of the reaction, the stirred reactor was cooled down to room temperature, and the stirrer was stopped. Gas was then



collected at the outlet of the reactor in a special cell for quantitative analysis of the partial pressure of reactant gases as well as the possible gas products (e.g., CO, methane, etc.). The catalyst was filtered out, and the liquid was collected for quantitative analysis. Blank measurement: a blank measurement without a catalyst was run for correcting the solvated CO₂ in water. Gas and liquid analysis is described in more detail in the ESI† part.

Characterization methods

See additional experimental details and supporting results in the ESI† part.

Conclusion

In summary, we demonstrated that a water-soluble, naturally occurring Cu-based porphyrin complex, chlorophyllin, can enhance the gas capture in water, which promotes the hydrogenation of CO₂ at the liquid/solid interface for Cu_xAu_y/ZnO catalysts. Clearly, the presence of the chlorophyllin complex did not result in any side products, and it was not found catalytically active for CO₂ hydrogenation in the absence of the solid Cu_xAu_y/ZnO catalyst. Based on zeta potential studies and spin-trap assisted EPR spectroscopy, the presence of chlorophyllin not only enhances CO₂ solubility in water but also promotes its electrostatic interactions with the surface. It further enhances the formation of C-centered and OH radicals during CO₂ hydrogenation. These findings pave the way for the development of hybrid systems that combine CO₂ capture and catalytic conversion in a single process and furthermore enhance our understanding of CO₂ interaction in the liquid phase with solid surfaces.

Data availability

The majority of raw data are included in the ESI† and any other data will be available upon request.

Author contributions

HM: synthesis, catalysis, zeta potential analysis and first draft; KN: SEM; MP: STEM; THV: EPR; AMA: project proposal, conceptualization, supervision, data curation, first draft, editing and revision. All authors read, revised and agreed on the submitted draft.

Conflicts of interest

The authors declare no known conflict of interest.

Acknowledgements

We thank Fr. Anja Simmula and Dr Henrik Lund/Fr. Kathleen Schubert for ICP-OES and PXRD measurements, respectively. We acknowledge the financial support from the Wissenschaftsgemeinschaft Gottfried-Wilhelm-Leibniz (WGL) in the frame of the SUPREME project (grant no. K308/2020).

Notes and references

- 1 R. Schlögl, *Angew. Chem., Int. Ed.*, 2022, **61**, e202007397.
- 2 G. A. Olah, *Angew. Chem., Int. Ed.*, 2013, **52**, 104–107.
- 3 G. A. Olah, *Catal. Lett.*, 2004, **93**, 1–2.
- 4 S. Zheng, Z. Zhang, S. He, H. Yang, H. Atia, A. M. Abdel-Mageed, S. Wohlrab, E. Baráth, S. Tin and H. J. Heeres, *Chem. Rev.*, 2024, **124**, 10701–10876.
- 5 R. Klaewkla, M. Arend and W. F. Hoelderich, in *Mass Transfer – Advanced Aspects*, IntechOpen, 2011, vol. 5, pp. 667–684.
- 6 J. Reichert, S. Maerten, K. Meltzer, A. Tremel, M. Baldauf, P. Wasserscheid and J. Albert, *Sustain. Energy Fuels*, 2019, **3**, 3399–3405.
- 7 X. Liu, S. Inagaki and J. Gong, *Angew. Chem., Int. Ed.*, 2016, **55**, 14924–14950.
- 8 S. Xie, W. Zhang, X. Lan and H. Lin, *ChemSusChem*, 2020, **13**, 6141–6159.
- 9 N. Liu, S. Bartling, A. Springer, C. Kubis, O. S. Bokareva, E. Salaya, J. Sun, Z. Zhang, S. Wohlrab and A. M. Abdel-Mageed, *Adv. Mater.*, 2024, **36**, 2309526.
- 10 J. Mosrati, T. Ishida, H. Mac, M. Al-Yusufi, T. Honma, M. Parlinska-Wojtan, Y. Kobayashi, A. Klyushin, T. Murayama and A. M. Abdel-Mageed, *Angew. Chem., Int. Ed.*, 2023, e202311340, DOI: [10.1002/anie.202311340](https://doi.org/10.1002/anie.202311340).
- 11 Murayama, T. Ishida, C. Mochizuki, A. M. Abdel-Mageed and R. J. Behm, *US Pat.*, 17/921,026, 2023.
- 12 Murayama, T. Ishida, C. Mochizuki, A. M. Abdel-Mageed and R. J. Behm, *Japan Pat.*, PCT/JP2021/015916, 2021.
- 13 K. Stangeland, H. Li and Z. Yu, *Ind. Eng. Chem. Res.*, 2018, **57**, 4081–4094.
- 14 S. Chen, A. M. Abdel-Mageed, A. Hauble, T. Ishida, T. Murayama, M. Parlinska-Wojtan and R. J. Behm, *Appl. Catal., A*, 2021, **624**, 118318.
- 15 A. M. Abdel-Mageed, M. Büsselmann, K. Wiese, C. Fauth and R. J. Behm, *Appl. Catal., B*, 2021, **297**, 120416.
- 16 A. M. Abdel-Mageed, A. Klyushin, A. Knop-Gericke, R. Schlögl and R. J. Behm, *J. Phys. Chem. Lett.*, 2019, **10**, 3645–3653.
- 17 D. Zhu, L. Wang, W. Yu and H. Xie, *Sci. Rep.*, 2018, **8**, 5282.
- 18 Q. Ren, L. Hao, J. Yang, M. Lv, H. Zhou, Z. Li, H. Duan and M. Shao, *ACS Catal.*, 2024, **14**, 5675–5684.
- 19 J. Yan, B. Zhang, S. Guo and Z. Wang, *ACS Appl. Nano Mater.*, 2021, **4**, 10565–10574.
- 20 R. Xiong and D. J. Keffer, *Renewable Sustainable Energy*, 2011, **3**(5), 053105.
- 21 A. M. Abdel-Mageed and S. Wohlrab, *Catalysts*, 2022, **12**, 16.
- 22 M. H. Habibi and B. Karimi, *J. Ind. Eng. Chem.*, 2014, **20**, 925–929.
- 23 A. Rezvani, A. M. Abdel-Mageed, T. Ishida, T. Murayama, M. Parlinska-Wojtan and R. J. r. Behm, *ACS Catal.*, 2020, **10**, 3580–3594.
- 24 R. Marsalek, *APCBEE Proc.*, 2014, **9**, 13–17.
- 25 M.-H. Liao, C.-H. Hsu and D.-H. Chen, *J. Solid State Chem.*, 2006, **179**, 2020–2026.
- 26 F. Yuan, H. Peng, Y. Yin, Y. Chunlei and H. Ryu, *Mater. Sci. Eng., B*, 2005, **122**, 55–60.



- 27 A. M. Abdel-Mageed, D. Widmann, S. E. Olesen, I. Chorkendorff and R. J. R. Behm, *ACS Catal.*, 2018, **8**, 5399–5414.
- 28 K. Wiese, A. M. Abdel-Mageed, A. Klyushin and R. J. Behm, *Catal. Today*, 2018, **336**, 193–202.
- 29 F. A. Villamena, E. J. Locigno, A. Rockenbauer, C. M. Hadad and J. L. Zweier, *J. Phys. Chem. A*, 2006, **110**, 13253–13258.
- 30 L. Li, X. Kang, M. He, A. Sheveleva, K. Hu, S. Xu, Y. Zhou, J. Chen, S. Sapchenko, G. Whitehead, I. J. Vitorica-Yrezabal, L. Lopez-Odrizola, L. S. Natrajan, E. J. L. McInnes, M. Schröder, S. Yang and F. Tuna, *J. Mater. Chem. A*, 2022, **10**, 17801–17807.
- 31 K. Qian, T. Wei, X. Yan, D. Qi, M. Tan and R. Li, *ACS Appl. Mater. Interfaces*, 2025, **17**, 12357–12374.
- 32 J. T. Feaster, C. Shi, E. R. Cave, T. Hatsukade, D. N. Abram, K. P. Kuhl, C. Hahn, J. K. Nørskov and T. F. Jaramillo, *ACS Catal.*, 2017, **7**, 4822–4827.

